01 Nov 2007

Estimation of High-Frequency Currents from Near-Field Scan Measurements

Haixiao Weng

Daryl G. Beetner
Missouri University of Science and Technology, daryl@mst.edu

Richard E. DuBroff
Missouri University of Science and Technology, red@mst.edu

Jin Shi

Recommended Citation

H. Weng et al., "Estimation of High-Frequency Currents from Near-Field Scan Measurements," *IEEE Transactions on Electromagnetic Compatibility*, vol. 49, no. 4, pp. 805-815, Institute of Electrical and Electronics Engineers (IEEE), Nov 2007.
The definitive version is available at https://doi.org/10.1109/TEMC.2007.908264

Estimation of High-Frequency Currents From Near-Field Scan Measurements

Haixiao Weng, *Member, IEEE*, Daryl G. Beetner, *Senior Member, IEEE*, Richard E. DuBroff, *Senior Member, IEEE*, and Jin Shi

***Abstract*—High-frequency currents on the pins of integrated circuits (ICs) and on printed circuit board (PCB) traces are needed to predict and analyze electromagnetic interference in high-speed devices. These currents can, however, be difficult to measure when traces are buried within the PCB or chip-package, especially when several current-carrying traces are in close proximity. Techniques for estimating high-frequency currents from near-field scan data are proposed in this paper. These techniques are applied to find currents on the pins of an IC, on traces buried beneath other traces in a PCB, and on traces over a slot in the ground plane. Methods of dealing with the ill-posed nature of the current-estimation problem are discussed, as are applications to electrically large structures. A study of the sensitivity of the technique to errors in the measured fields, errors in the circuit geometry, and errors in the estimated dielectric constant of the PCB or chip package show that, for reasonable errors in these parameters, currents can be estimated to within an average of 20% (1.6 dB) or less of their correct values.**

***Index Terms*—Compensation, current measurement, estimation, inverse problems, magnetic field measurement.**

I. Introduction

INCREASING clock frequencies, communication speeds, and edge rates are making design for electromagnetic compatibility (EMC) increasingly difficult. Measuring high-frequency voltages and currents is critical to finding and predicting the cause of EMC problems. Many techniques exist to measure currents and voltages [1]–[6], but each has its drawbacks. For example, the 1-Ω method measures conducted high-frequency currents by inserting a 1-Ω resistor in series with the circuit and measuring the voltage across it. The 150-Ω method measures high-frequency voltage using a 150-Ω coupling network. Transverse electromagnetic (TEM)-cell measurements gauge the ability of an integrated circuit (IC) to couple electrically or magnetically to nearby structures. The 1- and 150-Ω methods both require special alterations to the circuit that may modify the characteristics of the noise signal. All three techniques require special test boards, which may not be practical or desirable when working with "real" circuits. In some instances, where traces or vias are available on the exposed surfaces of the printed circuit board (PCB), the "real" board can be modified to apply the 1- or 150-Ω measurements, though difficulties still exist when vias and traces are buried within the PCB.

High-frequency currents may also be measured using the magnetic-probe method. The magnetic field strength close to a pin or trace is measured using a noncontact miniature magnetic probe [2]–[5]. The current is calculated based on the characteristics of the probe, its position relative to the circuit, and the circuit geometry [5]. An advantage of this technique is that it has minimal impact on the circuit under test and can be used with "real" circuits, even when traces are hidden, without the creation of special test boards. The resolution of this method, however, is highly dependent on the geometry and position of the probe. The extremely small pitch between pins and traces in modern circuits may cause interference from one trace to another, reducing the accuracy of the measurement. Pins hidden beneath the package in a ball-grid array may be particularly problematic, since the magnetic field probe cannot be placed right next to the pin. Using an extremely small magnetic probe can minimize the influence from other pins or traces when one can get very close to the pin or trace of interest, but the sensitivity of such a probe is low and is not typically suitable for time-domain measurements.

Another approach to measuring high-frequency currents and voltages is using near-field scans [7]–[9]. With this approach, the orientation and intensity of electromagnetic fields close to an IC or PCB are found by measuring the electric or magnetic field at well-defined intervals about the device, typically in a plane just above the circuit. Near-field scans are useful for discovering "hot spots" within the circuit and approximating the flow of high-frequency currents. A near-field scan does not require a special test board or modifications to an existing circuit, though currents are not measured directly and interference between closely spaced pins or traces may limit the resolution of the technique. The measured near-electric and magnetic fields might also be used to infer the size and position of high-frequency currents. Similar data are used to estimate the currents in a trace or pin in the IEC Standard 61967-6 [5] or to estimate equivalent sources representing the electrical activity of the heart [10]–[12].

In this paper, methods are developed to estimate currents flowing within a chip package or within traces hidden within a PCB. Experiments to validate this approach are performed to predict currents in a simple circuit, currents within the pins of a clock buffer chip, currents in traces hidden within a PCB, and currents in traces over a slot in the ground plane. Inherent issues of stability and susceptibility to measurement error of the inverse problem are also discussed.

Manuscript received June 7, 2006; revised December 12, 2006.

H. Weng is with Texas Instruments, Inc., Dallas, TX 75266-0199 USA (e-mail: haixiao.weng@ti.com).

D. G. Beetner and R. E. DuBroff are with the Department of Electrical and Computer Engineering, University of Missouri-Rolla, Rolla, MO 65409 USA (e-mail: daryl@mst.edu; red@mst.edu).

J. Shi is with the Electromagnetic Compatibility Laboratory, University of Missouri-Rolla, Rolla, MO 65409 USA, and also with the Intel Corporation, Santa Clara, CA 95054-1549 USA (e-mail: jin.shi@intel.com).

Color versions of one or more of the figures in this paper are available online at http://ieeexplore.ieee.org.

Digital Object Identifier 10.1109/TEMC.2007.908284

II. Theory

Unknown currents in a chip or PCB can be represented using a distribution of current dipoles $\vec{J}(\omega, x, y, z)$, where ω is the angular frequency and $x, y,$ and z are coordinate positions. The relationship between the unknown currents and the measured fields may be calculated using the Green's function. As the currents in a chip or board are typically operating over a ground plane, both the current and its image should be taken into account.

Consider a set of current sources in a volume V in free space, where all locations $z > z'$ are source-free. The magnetic field in the source-free area $\vec{H}(\omega, x, y, z)$ is given by [13]

$$\begin{aligned}\vec{H}(\omega,x,y,z) = \hat{x}\oint_{V'}&[J_y(x',y',z')(z-z')\\&-J_z(x',y',z')(y-y')]G_{12}\,dV'\\&+\hat{y}\oint_{V'}[J_z(x',y',z')(x-x')\\&-J_x(x',y',z')(z-z')]G_{12}\,dV'\\&+\hat{z}\oint_{V'}[J_x(x',y',z')(y-y')\\&-J_y(x',y',z')(x-x')]G_{12}\,dV' \qquad (1)\end{aligned}$$

where

$$G_{12} = \frac{(1+ikR)\,e^{-ikR}}{4\pi R^3} \qquad (2)$$

$\vec{r}' = x'\hat{x} + y'\hat{y} + z'\hat{z}$ represents the location of the source current, $\vec{r} = x\hat{x} + y\hat{y} + z\hat{z}$ represents the location of the field point, $R = \sqrt{(x-x')^2 + (y-y')^2 + (z-z')^2}$ is the distance between the source point and the field observation point, k is the wavenumber, $\vec{J}(\omega, x', y', z') = J_x\hat{x} + J_y\hat{y} + J_z\hat{z}$ is the current source in the source volume V, and the source-free area is assumed to be in free space. The relationship between the source currents and the magnetic field can be discretized as

$$TJ = H \qquad (3)$$

where J and H are vectors describing the source currents and magnetic fields at discrete points in the source and source-free regions, respectively, and T is a transfer matrix defining the relationship between them. For our problem, J represents the unknown currents in an IC package or PCB and H represents the measured magnetic field in a plane above the device under test.

Using (3), unknown currents may be calculated from the measured magnetic field using the minimum least-squares residual

$$J = \left[T^T T\right]^{-1} T^T H. \qquad (4)$$

Such unconstrained inverse solutions are, however, inherently unstable [11]. Small errors in geometry or field measurements and limitations in sampling resolution can lead to large errors in inferred currents [14]. Regularization constraints must be placed on solutions for reasonable results. Constraints can include restrictions on the number or location of current sources (e.g., known trace geometry), restrictions on the rate of change of current magnitudes, and others [11]. One constrained, or regularized, solution for (4) is to find the currents J that minimize the function

$$R_\gamma = \|H - TJ\|^2 + \gamma\,\|CJ\|^2 \qquad (5)$$

where C is a constraint matrix and γ is a constant "regularization parameter" that controls the weight attributed to the constraint condition [11].

In this paper, knowledge about the lead frame, trace geometry, or PCB was used to constrain solutions by limiting the number, location, and direction of possible current sources. The constraint matrix C was designed such that $\|CJ\| = 0$ when currents flow in a single direction in a known trace, so that currents in a trace are considered as one source instead of many separate current dipoles. Currents were assumed to be zero where there is no known current path; for example, where there is no metal in the PCB. Where the possible current paths are not clear or are too dense for a simple solution; for example, in the silicon die, solutions were constrained by describing them using a grid of current dipoles, as shown in Fig. 1, thus constraining both the number and location of the sources at the possible expense of resolution. Other constraints, such as load information, could also be placed on the solution, but were not explored here.

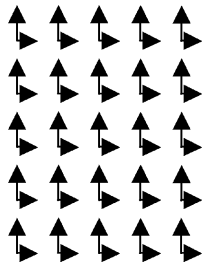

Fig. 1. Network of inferred current dipoles.

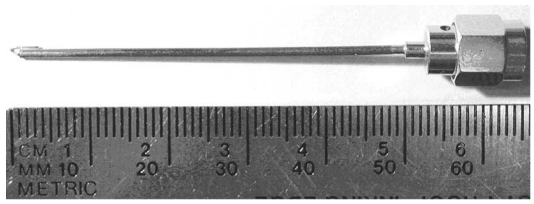

Fig. 2. Magnetic field loop probe.

III. Methods

The ability to estimate currents from near-field scan data was tested by measuring and compensating the near-magnetic field over a simple circuit, over an IC, and over traces in a PCB and, then, predicting the currents in those circuits. The near-magnetic field was measured using the loop probe shown in Fig. 2. The loop was approximately 0.7 mm in diameter. Its center was placed approximately 1.7 mm above the circuit during measurement. Scanning was performed using the setup shown in Fig. 3. Measurements were made with a network analyzer or an oscilloscope to measure phase. Because of the low sensitivity of the probe, a 25-dB preamplifier was connected between the probe and the oscilloscope or network analyzer. The

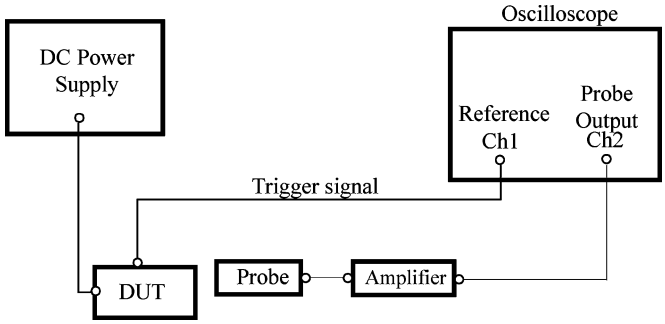

Fig. 3. Typical setup for measuring the near-magnetic field.

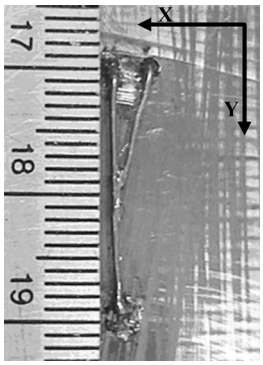

Fig. 4. Photograph of circuit.

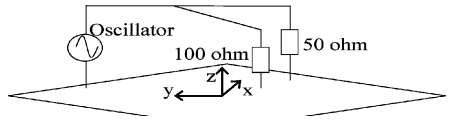

Fig. 5. Experimental setup.

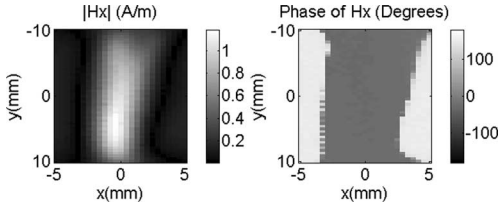

Fig. 6. Compensated magnetic field.

TABLE I
CALCULATED AND ESTIMATED CURRENT AT 100 MHZ

Trace with load	Recovered Current at 100 MHz (mA)	
	From Ohm's law	From the measured field
50 Ω	11.1	11.6
100 Ω	5.6	5.8

characteristics of the amplifier and cable were calibrated using a network analyzer. A dual-probe approach, where a second loop probe was placed close to the device under test to generate a trigger signal, was used to synchronize measurements made at different locations when measuring free-running circuits with the oscilloscope [15].

Because the size of the loop probe was small compared to the size of and distance from the circuit under test, the magnetic field measured by the probe could be approximated from the measured voltage as

$$\vec{H} = \frac{V}{j2\pi f S \mu_0} \tag{6}$$

where $\vec{H}$ is the compensated magnetic field, V is the voltage measured by the oscilloscope or network analyzer, f is the frequency, S is the area of the loop probe, and μ_0 is the permeability of free space. For larger probes or more accurate measurements, the probe output should be calibrated and compensated as described in [16].

A. Estimation of Current in a Simple Circuit

The current estimation procedure was first tested on the simple circuit shown in Figs. 4 and 5. The circuit consisted of a 100-MHz oscillator feeding two loads (50 and 100 Ω) through wires suspended 2.5 mm over a ground plane. The magnetic field over the circuit was scanned over a 49 × 25 grid of sample points covering a 2 cm × 1 cm area (y- and x-directions, respectively). Fig. 6 shows the compensated magnetic field in the x-direction based on probe measurements at 100 MHz. Fields are calculated from the fast Fourier transform (FFT) of the measured time-domain signal. Note that while the general location and relative magnitude of currents are recognizable, many details are hidden by the spatial filtering inherent to the measurement.

1) Estimation of Current Using Trace Geometry: In the first experiment, the wire geometry was assumed to be known and was used to constrain solutions for current. Since the circuit is electrically small, current is constant along the trace, and the circuit may be represented using three current sources: one for the wire leading to the 50-Ω load, one for the 100-Ω resistor, and one for the wire connected to the oscillator. Each source completely represented the wire geometry.

The magnitudes of the currents were estimated at 100 MHz and at its harmonics up to 1 GHz. Table I shows the estimates at 100 MHz. The estimated currents were compared to the currents measured in the 50- and 100-Ω loads by measuring the voltage drop across them with a 25-to-1 probe and calculating current using Ohm's law. The difference between the measured and the estimated currents was small (i.e., maximum error 13%, average error 6%) at all the frequencies. A comparison between the measured and the estimated time-domain currents through the 100-Ω load (Fig. 7) shows a maximum difference of less than 2 mA out of an approximate 25-mA range (i.e., maximum error less than 8%).

2) Estimation of Current Without Trace Geometry: Using trace geometry to constrain solutions gives the best chance of producing reasonable estimates of current, but the trace geometry may not always be known. Estimates of currents may still be made using the grid of current sources shown in Fig. 1. To illustrate, currents in the simple circuit (Fig. 4) were found for a 21 × 11 grid of current sources. The resulting estimates of currents shown in Fig. 8 are not as accurate as those found when

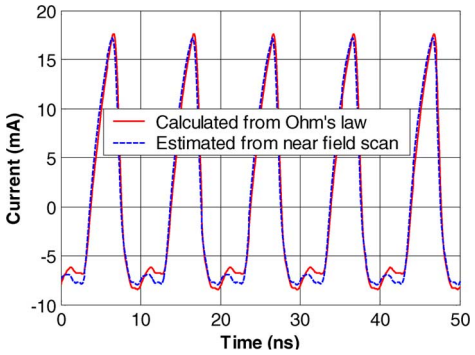

Fig. 7. Estimated time-domain current through the 100-Ω load.

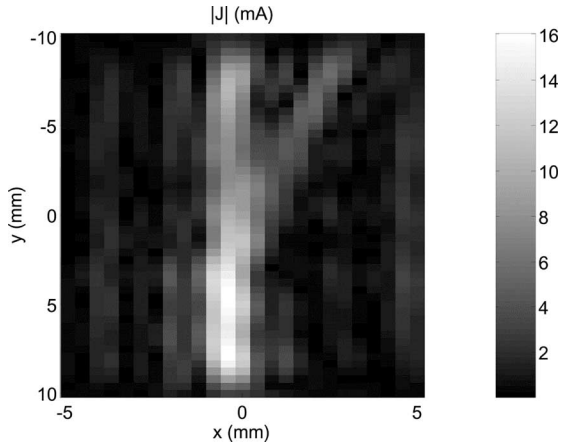

Fig. 8. Estimated matrix of current dipoles.

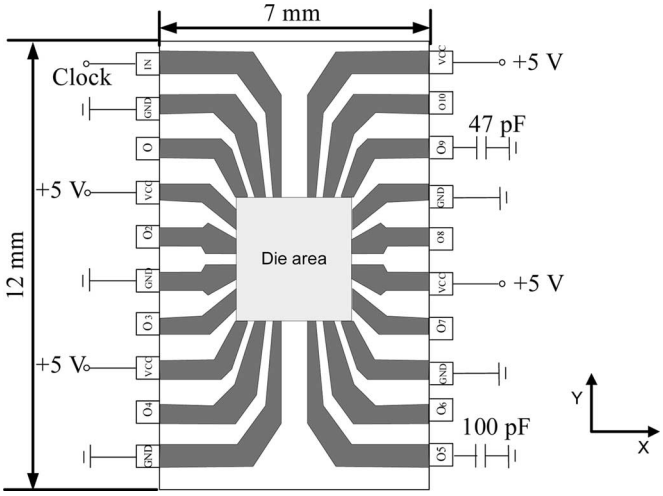

Fig. 9. Lead frame for the clock driver and connections to external circuit.

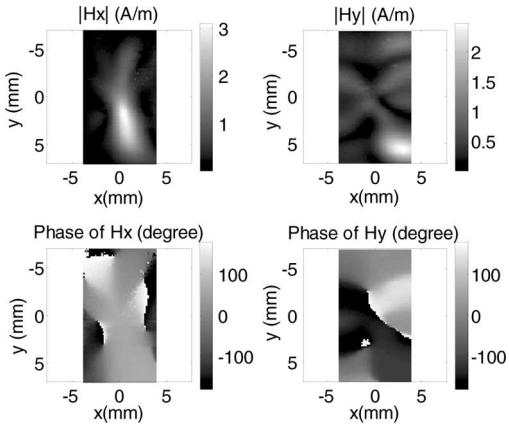

Fig. 10. Compensated magnetic field over the clock buffer.

using the exact trace geometry, but show significantly more detail about the location and magnitude of currents than is apparent from the near-magnetic field scan without processing, as shown in Fig. 6.

B. Estimation of Currents in the Package of a Clock Driver

Currents within the lead frame of an active IC, specifically a 1-to-10 clock driver (IDT74FCT807BT/CT) [17] were also estimated from near-magnetic field scans. The lead frame and its connections to the PCB are illustrated in Fig. 9. A 100-MHz clock input was fed to the driver through pin 1 on the top left corner of the chip. Outputs 5 and 9 (pins 11 and 18) drove 47- and 100-pF loads. All other outputs were left floating. The chip package held the lead frame approximately 1.2 mm above the solid return plane of the PCB. A 49 × 89 point near-field scan was made across the chip over a 13.97 mm × 7.62 mm area (y- and x-directions, respectively). The compensated magnetic field based on probe measurements at 100 MHz is shown in Fig. 10. Here again, while important information is contained within the near-field scan, it is often difficult to discern the precise magnitude of currents or where they flow.

The geometry of the lead frame was used to constrain solutions for the current sources. A single current source was defined for each of the 20 leads in the lead frame. Each source completely represented the lead geometry. For the die in the center of the lead frame, however, the current path geometry could not be well defined. To estimate currents in the die area, the 3.6 mm × 3.6 mm die was divided into nine 1.2 mm × 1.2 mm patches. A single x-directed and y-directed current source was estimated for each patch, using a grid similar to Fig. 1. A total of 38 currents were estimated for the chip.

To determine the accuracy of the estimated currents, currents in package pins were measured using a special-purpose coaxial cable probe [18]. The probe is made from a coaxial cable with a small slot cut in one side that allows magnetic fields very close to the slot to couple inside the cable. This probe allows high spatial resolution measurement of magnetic fields produced by individual pins, even when the pins are very close to one another.

The normalized 100-MHz currents measured using the slotted coaxial cable probe and estimated from near-field scans are shown in Fig. 11. The currents are normalized to the maximum current found in each case because the slotted cable probe produces a good measure of the relative size of currents, but it is difficult to find their precise magnitude. The normalized measured and estimated currents are within approximately 10% of one another. The time-domain current through the 47-pF capacitor was also found from the inverse FFT, as shown in Fig. 12. In this case, currents through the capacitor were calculated from

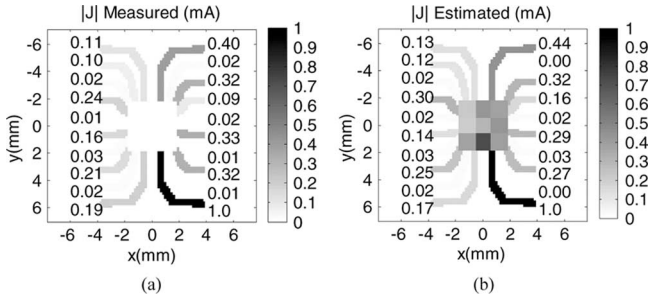

Fig. 11. Measured and estimated current flowing in the clock buffer. The magnitude of currents in the lead frame is shown next to the pins.

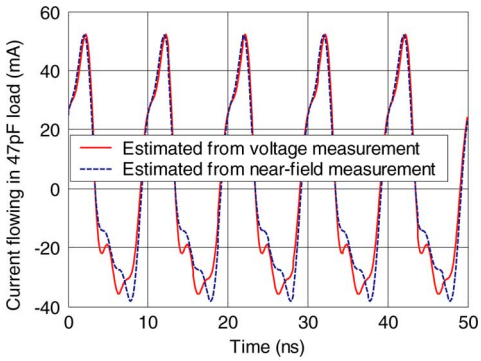

Fig. 12. Estimated current through 47-pF load in time domain.

a measurement of the voltage drop across the capacitor. Maximum errors over time were less than 10 mA over an approximate 100-mA range (i.e., less than 10%).

There are several possible reasons for differences between the measured and the estimated currents. One possibility is that the scalar calibration and compensation technique used here may not be adequate for this application. In particular, capacitive coupling between the device and the probe may influence results. Random or systematic errors in the measurements, for example, accurate placement of the device relative to the probe or accurate measurement of the angular rotation of the probe (which is determined by the eye), may also induce errors in the inferred values of current. Another possibility is that multiple reflections between the lead-frame and the ground plane are more significant than anticipated. These reflections are not accounted for in the present model. Some of these sources of error are explored further in the discussion.

C. Estimation of Currents in Traces Over a Slot in the Ground Plane

In the previous applications, a solid ground plane was assumed and the transfer coefficient matrix was easily calculated using closed-form solutions. When a gap exists in the ground plane, the relationship between the currents and the measured magnetic fields is more complicated. The relationship, however, can still be calculated using a numerical solution. In the following example, currents flowing in three traces over a gap in the ground plane were recovered from the near-field measurement. The traces and ground plane are shown in Fig. 13. The traces

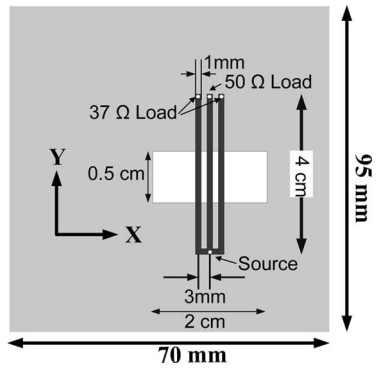

Fig. 13. Traces over a slot in the ground plane.

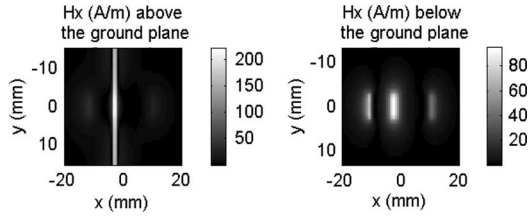

Fig. 14. Magnetic field calculated for the left trace, 0.6 mm above and below the ground plane, using a TLM solver.

are 4 cm long, 1 mm wide, and 3 mm apart. The return plane beneath the traces is interrupted by a 2 cm × 0.5 cm slot. At one end, the traces were shorted together and, at the other end, they were terminated with 37-, 50-, and 37-Ω loads to the ground.

A 101 × 141 point near-field scan was made over a 2 cm × 4 cm area (y- and x-directions, respectively) using a network analyzer. Port 1 of the network analyzer was connected to the source end of the traces shown in Fig. 13 while port 2 was connected to the probe. Since the slot in the ground plane allowed the fields from the traces to be visible on both sides of the board, measurements were performed both above and below the slot (i.e., on the same side as the trace and on the opposite side from the trace, respectively).

The transfer coefficient matrix relating the currents in the traces to the magnetic fields were calculated using the FloEMC transmission line solver. For example, Fig. 14 shows the calculated relationship between the leftmost trace and the measured magnetic field both above and below the ground plane. The simulations show the field at 100 MHz, 0.6 mm from the ground plane. These calculations were used to form the transfer coefficient matrix. Similar relationships were calculated for the other traces. To minimize the possibility that the use of simulated rather than measured data might skew results, calculations of the transfer coefficients and currents were repeated with the HFSS finite-element tool and compared to results with the FloEMC transmission line solver for each structure tested. The two simulation results agreed within 2% or less, indicating that the simulated data should be reliable.

Table II shows the currents estimated in each trace through simulation, estimated from the near-field scan measurement above the ground plane, and estimated from the near-field scan measurement below the ground plane. Maximum errors were less than 10% of the total current. The current could be estimated

TABLE II
RECOVERED CURRENT FOR EACH TRACE

Trace	From simulation	From the field measured above the ground plane	From the field measured below the ground plane
Left Trace	5.7	5.4	5.2
Center Trace	4.3	4.3	4.5
Right Trace	5.7	5.6	5.2

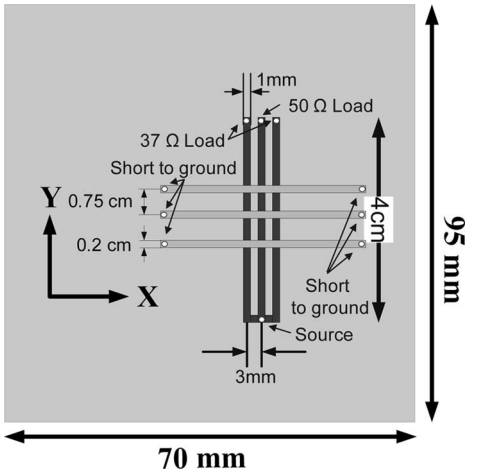

Fig. 15. Traces crossing one another in a PCB. Currents were estimated in the vertical traces, which are buried within the PCB.

slightly better using measurements above the ground plane, on the same side as the trace, than using measurements below the ground plane, though both measurements gave reasonable results.

D. Estimation of Currents in Buried Traces

While the current in an exposed trace or pin may be measured using a magnetic probe [19], this technique may have trouble when traces are hidden within the PCB, especially if the traces are very close to one another or close to other strong current sources. To test the ability of this technique, the currents were estimated in three traces buried within a PCB beneath three other traces, as shown in Fig. 15. The traces are backed by a ground plane on the bottom layer. Each plane in the PCB is separated by 1 mm of FR4. The traces on the top layer are connected to the ground plane. The three buried traces are connected as in Section III-C. Measurement and simulation of fields and currents were performed as in Section III-C. The currents estimated from the compensated magnetic field measurement are shown in Table III. Maximum error between the simulated and the estimated currents was less than 10% of the total current.

E. Estimation of Currents in an Electrically Large Trace

In the previous examples, the current flowing in a trace was assumed to be the same everywhere because the trace was electrically small. Displacement current cannot be ignored, however, once the frequency is high and the trace becomes electrically large. If this happens, the current can be modeled as a summation of a forward and a backward wave as

$$I = I^{+}e^{j\beta l} + I^{-}e^{-j\beta l} \tag{7}$$

TABLE III
RECOVERED CURRENT IN BURIED TRACES

Trace	Recovered Current/Source Voltage (mA/V)	
	From simulation	From the measured field
Left Trace	5.7	5.4
Center Trace	4.3	4.2
Right Trace	5.7	5.7

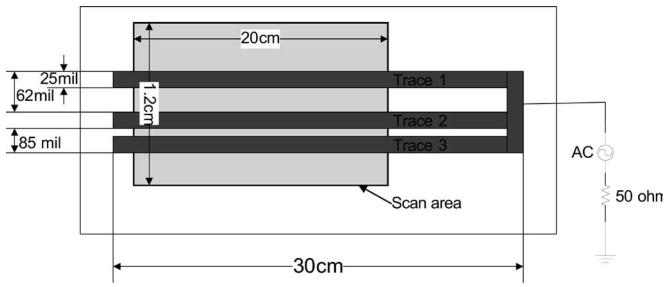

Fig. 16. Structure used to test the estimation of current when circuit geometries are electrically large.

where I^{+} is the forward current, I^{-} is the backward current, l is the distance from the load resistor, and β is the wavenumber. The ratio of the forward and backward currents is given by the reflection coefficient

$$\frac{I^{-}}{I^{+}} = -\Gamma_L = -\frac{Z_L - Z_0}{Z_L + Z_0} \tag{8}$$

where Z_L is the load impedance and Z_0 is the characteristic impedance of the trace. The current along the trace can be estimated from the near-field scan as before, except for two unknowns, I^{+} and I^{-}, which are estimated instead of just one. The estimate can be improved with *a priori* knowledge of Γ_L.

This model was used to estimate the currents in the traces shown in Fig. 16. The traces are 30 cm long, 25 mil wide, and 15 mil above a ground plane, and the permittivity, ε_r, of the PCB is 4.4, so the traces are electrically large for frequencies greater than 75 MHz (trace length greater than a quarter wavelength). The traces are terminated on one end with a 68-Ω resistor and have a characteristic impedance of 53 Ωs, giving a reflection coefficient of $\Gamma_L = 0.124$. The traces are driven on the other end, where they are connected together, through a 50-Ω series impedance so that reflections are negligible at this end. Measurements were performed at 500 MHz, where the wavenumber is $\beta = 17.1$ rad/m (the speed of light in the microstrip trace is about 1.8×10^8 m/s).

The near-field scan was performed over a 20 cm × 1.2 cm (201 × 61 point) area over the traces. Measurements were made using a network analyzer as before. Currents in the traces were also calculated using transmission line theory. Fig. 17 shows the estimated and simulated currents in the traces as a function of position, when currents were estimated without any knowledge of the impedance associated with the trace. The maximum error between the currents estimated from the near field scan and the simulated currents is less than 8%. The magnitude and the phase of the estimated currents improve when given the value of Γ_L, as shown in Fig. 18, where maximum errors are less than 7%.

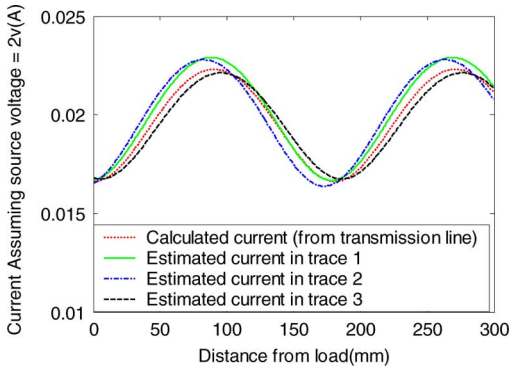

Fig. 17. Estimated current in electrically large traces when reflection coefficient was not known.

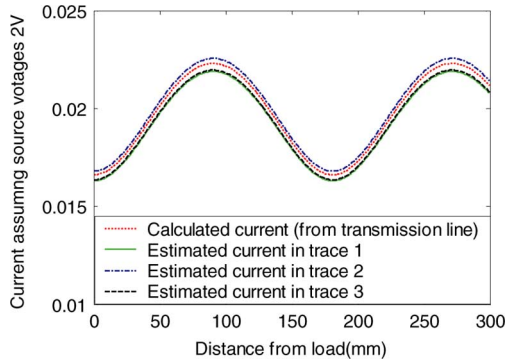

Fig. 18. Estimated current in electrically large traces when the reflection coefficient was known.

IV. Accuracy of Estimated Currents

The accuracy of estimated currents is particularly dependent on the accuracy of assumptions and measurements because of the ill-posed nature of the inverse problem. Errors in the position of the probe relative to the device under test, errors in the rotational orientation of the probe, random noise in the measured fields, and errors in the assumed dielectric constant of the medium may all influence the accuracy of the result. To show the effect of these errors, currents were estimated when these errors were intentionally incorporated into the measured data and a theoretical study of each error type was performed. First, an experiment was performed using the clock driver data shown in Fig. 11. The magnetic field 1.7 mm above the surface of the IC was calculated from the currents estimated in the previous study. New currents were inferred from these magnetic fields assuming a 0.2-mm error in the horizontal position of the probe (relative to the device under test), a 0.2-mm error in the probe height (vertical position), a 15° error in the assumed rotational position of the probe, and with 10% random noise added to the measured fields (i.e., the average amplitude of the random noise was 10% of the average amplitude of the measured signal). These errors are typical of what one might expect with the equipment we use to perform near-field scans. The results of the simulations are summarized in Table IV and the errors in the current estimations ranged from about 6 to 18.3%. While errors in the vertical height of the probe were found to be important, the probe height can, often, be controlled well (i.e., within less than a 0.2-mm error) by bringing the probe down to touch the surface of the device under test and, then, backing it away using stepper motors.

TABLE IV
Average Error in Inferred Currents

	Error in measurement			
	0.2 mm error in horizontal position	0.2 mm error in height	15° error in rotational position	10% random noise
Error in inferred currents	7.3%	18.3%	11.3%	5.9%

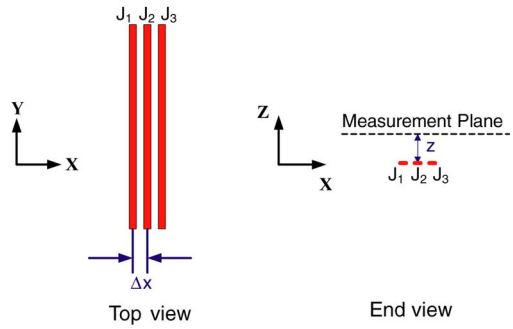

Fig. 19. Structure used to test the influence of uncertainty in the estimation.

To further quantify errors that might be expected in inferred currents, a theoretical study was performed on the simple three-trace structure shown in Fig. 19. The three traces are located in the z-plane ($z = 0$), are infinitely long in the y-direction, are parallel to the y-axis, and cross the x-axis at positions $x = -\Delta x, x = 0$, and $x = \Delta x$. Currents J_1, J_2, and J_3 flow through the traces. Scanning is assumed to take place perpendicular to the three traces, along the x-axis, at height $z = z_p$.

If magnetic fields are measured with an error in position, the relationship between the fields and the currents in the traces is given by

$$H' = T'J \tag{9}$$

where H' is a vector of the fields measured at the wrong position and T' is the transfer coefficient matrix that relates those fields to the current sources. From (4), the currents inferred from these incorrect magnetic fields using the original transfer coefficient matrix (since the error is unknown) are given by

$$J' = \left[T^T T\right]^{-1} T^T H' = \left[T^T T\right]^{-1} T^T T' J \tag{10}$$

where J' are the currents inferred from the incorrect geometry. The error between the correct currents, J, and the currents inferred from the incorrect geometry J' is given by

$$J' - J = \left[\left[T^T T\right]^{-1} T^T T' - I\right] J. \tag{11}$$

Errors in the inferred currents can, then, be expressed as

$$|J' - J| = \begin{bmatrix} \mathrm{ERR}_{11} & \mathrm{ERR}_{12} & \mathrm{ERR}_{13} \\ \mathrm{ERR}_{21} & \mathrm{ERR}_{22} & \mathrm{ERR}_{23} \\ \mathrm{ERR}_{31} & \mathrm{ERR}_{32} & \mathrm{ERR}_{33} \end{bmatrix} \begin{bmatrix} J_1 \\ J_2 \\ J_3 \end{bmatrix} \tag{12}$$

where ERR_{mn} gives the error in inferred current J'_m resulting from current J_n. The errors resulting from incorrect geometry, then, can be understood through analysis of $T^T T$ and $T^T T'$.

The transfer coefficient matrix T is given by

$$T = \begin{bmatrix} T_{11} & T_{12} & T_{13} \\ T_{21} & T_{22} & T_{23} \\ \vdots & \vdots & \vdots \\ T_{N1} & T_{N2} & T_{N3} \end{bmatrix}. \tag{13}$$

Since the measured magnetic field from the traces in the x-direction, $H_x(x, z_p)$, is given by

$$H_x(x, z_p) = \frac{z_p}{2\pi\left[(x+\Delta x)^2 + z_p^2\right]} J_1 + \frac{z_p}{2\pi\left[x^2 + z_p^2\right]} J_2 + \frac{z_p}{2\pi\left[(x-\Delta x)^2 + z_p^2\right]} J_3 \tag{14}$$

the coefficients of the transfer matrix are given by

$$T_{n1} = \frac{z_p}{2\pi\left[(x(n)+\Delta x)^2 + z_p^2\right]} \tag{15}$$

$$T_{n2} = \frac{z_p}{2\pi\left[x^2(n) + z_p^2\right]} \tag{16}$$

$$T_{n3} = \frac{z_p}{2\pi\left[(x(n)-\Delta x)^2 + z_p^2\right]} \tag{17}$$

where $x(n)$ is the position of the sample n along the x-axis. Assuming the sample density is high enough to allow coefficients of $T^T T$ to be calculated through integration along x and samples are taken far enough away from the source locations that additional samples will have negligible contribution, then

$$\left[T^T T\right] \approx \frac{N}{8\pi z_p L} \begin{bmatrix} 1 & \frac{4z_p^2}{\left[\Delta x^2+4z_p^2\right]} & \frac{z_p^2}{\left[\Delta x^2+z_p^2\right]} \\ \frac{4z_p^2}{\left[\Delta x^2+4z_p^2\right]} & 1 & \frac{4z^2}{\left[\Delta x^2+4z_p^2\right]} \\ \frac{z_p^2}{\left[\Delta x^2+z_p^2\right]} & \frac{4z_p^2}{\left[\Delta x^2+4z_p^2\right]} & 1 \end{bmatrix} \tag{18}$$

where N is the total number of sample points and L is the length of integration (L/N is the sample density).

If there is an error, e_x, in the x-position of the probe, then the transfer coefficients representing this error are given by

$$\begin{cases} T'_{n1} = \frac{z_p}{2\pi\left[(x(n)+e_x+\Delta x)^2+z_p^2\right]} \\ T'_{n2} = \frac{z_p}{2\pi\left[(x(n)+e_x)^2+z_p^2\right]} \\ T'_{n3} = \frac{z_p}{2\pi\left[(x(n)+e_x-\Delta x)^2+z_p^2\right]}. \end{cases} \tag{19}$$

Assuming the sampling density is high enough to allow coefficients of $T^T T'$ to be calculated through integration, $T^T T'$ for an x-direction error in probe position is given by

$$\left[T^T T'\right] \approx \frac{N}{8\pi z_p L} \times \begin{bmatrix} \frac{4z_p^2}{\left[(e_x)^2+4z_p^2\right]} & \frac{4z_p^2}{\left[(\Delta x-e_x)^2+4z_p^2\right]} & \frac{4z_p^2}{\left[(2\Delta x-e_x)^2+4z_p^2\right]} \\ \frac{4z_p^2}{\left[(\Delta x+e_x)^2+4z_p^2\right]} & \frac{4z_p^2}{\left[(e_x)^2+4z_p^2\right]} & \frac{4z_p^2}{\left[(\Delta x-e_x)^2+4z_p^2\right]} \\ \frac{4z_p^2}{\left[(2\Delta x+e_x)^2+4z_p^2\right]} & \frac{4z_p^2}{\left[(\Delta x+e_x)^2+4z_p^2\right]} & \frac{4z_p^2}{\left[(e_x)^2+4z_p^2\right]} \end{bmatrix} \tag{20}$$

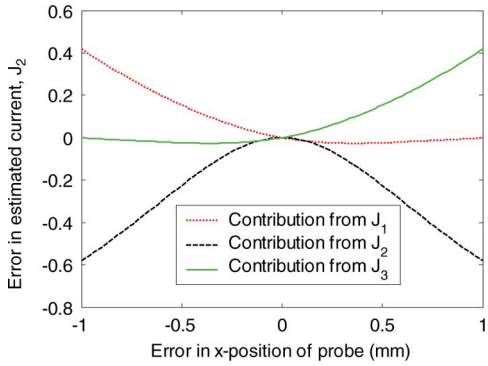

Fig. 20. Contribution of J_1, J_2, and J_3 to error in inferred current J'_2 as a function of probe alignment error in the x-direction.

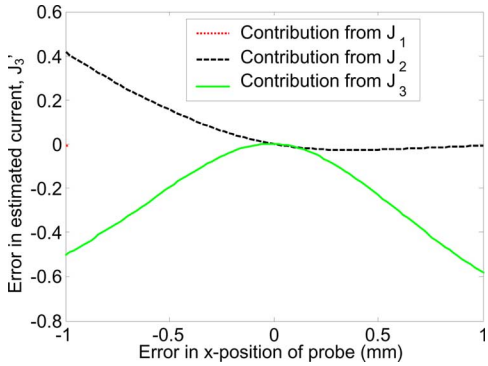

Fig. 21. Contribution of J_1, J_2, and J_3 to error in inferred current J'_3 as a function of probe alignment error in the x-direction.

which shows the error in the inferred currents J'_2 and J'_3 for an error in the x-direction of the probe. Since each true current, J_1, J_2, and J_3, will contribute differently to the error, plots show the relative contribution of each current to the error. Due to the symmetry of the test setup, errors for J_1 and J_3 are mirror images of one another. Not surprisingly, J_1 does not contribute significantly to errors in J_3 and vice versa. The default trace spacing and probe height used in these and the following figures are: $\Delta x = 2\,\mathrm{mm}$ and $z_p = 0.5\,\mathrm{mm}$, though other trace spacing and probe heights may be calculated easily. In general, the larger the spacing between traces and the lower the probe height, the smaller the error.

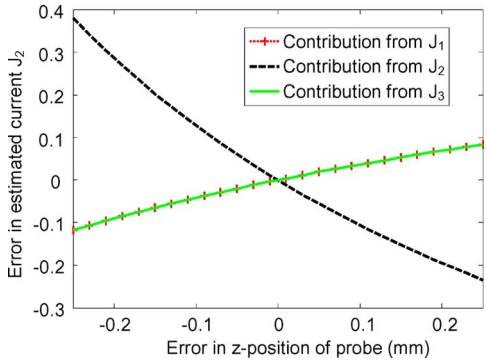

Fig. 22. Contribution of J_1, J_2, and J_3 to error in inferred current J_2' as a function of probe alignment error in the z-direction.

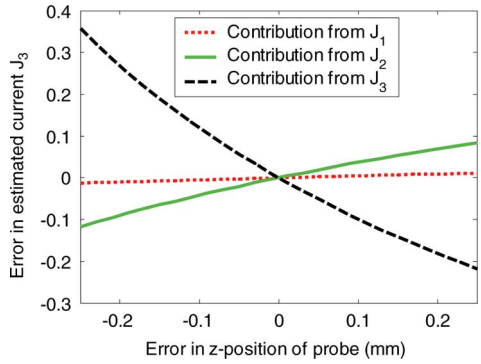

Fig. 23. Contribution of J_1, J_2, and J_3 to error in inferred current J_3' as a function of probe alignment error in the z-direction.

Transfer coefficients for an error, e_z, in the height of the probe (relative to the device under test) are given by

$$\begin{cases} T'_{n1} = \frac{(z_p+e_z)}{2\pi\left[(x(n)+\Delta x)^2+(z_p+e_z)^2\right]} \\ T'_{n2} = \frac{(z_p+e_z)}{2\pi\left[(x(n))^2+(z_p+e_z)^2\right]} \\ T'_{n3} = \frac{(z_p+e_z)}{2\pi\left[(x(n)-\Delta x)^2+(z_p+e_z)^2\right]}. \end{cases} \tag{21}$$

Again, assuming the sampling density is high enough to allow coefficients of $T^T T'$ to be calculated through integration, coefficients of $T^T T'$ for a vertical error in the probe position are given in (22), shown at the bottom of the page, where $a = -1,\ 0,\ +1$ for $i = 1,\ 2,\ 3$ and $b = -1,\ 0,\ +1$ for $j = 1,\ 2,\ 3$, respectively. Using this equation and (18), Figs. 22 and 23 were calculated to show the error contributed to inferred currents J_2' and J_3' by each current source as a function of error in the height of the probe.

If the assumed rotational position of the probe is in error by θ°, then

$$\begin{cases} T'_{n1} = \frac{z_p \cos\theta}{2\pi\left[(x(n)+\Delta x)^2+z_p^2\right]} \\ T'_{n2} = \frac{z_p \cos\theta}{2\pi\left[(x(n))^2+z_p^2\right]} \\ T'_{n3} = \frac{z_p \cos\theta}{2\pi\left[(x(n)-\Delta x)^2+z_p^2\right]} \end{cases} \tag{23}$$

giving $\left[T^T T\right]^{-1}\left[T^T T'\right] = \cos\theta$ for a dense sample spacing in the x-direction. In this case, an error of θ would cause inferred currents to be off by a factor of $(1-\cos\theta)$.

To find the influence of random noise in the measured fields, the uncertainty in the measured magnetic field at each point is assumed to be an independent Gaussian distributed random variable with a mean 0 and variance σ^2. The vector of the magnetic field errors is given by ΔH. The error in the inferred currents, ΔJ, caused by the errors in the field values is then

$$\Delta J = \left[T^T T\right]^{-1} T^T \left[\Delta H\right]. \tag{24}$$

To simplify equations, assume

$$\left[T^T T\right]^{-1} = \frac{L}{N}\begin{bmatrix} a_{11} & a_{12} & a_{13} \\ a_{21} & a_{22} & a_{23} \\ a_{31} & a_{32} & a_{33} \end{bmatrix}. \tag{25}$$

The error in the estimated current i is then

$$\begin{aligned} \Delta J_i = \sum_{n=0}^{N} \Bigg[& a_{i1} \cdot \frac{1}{\left[(x(n)+\Delta x)^2 + z_p^2\right]} \\ & + a_{i3} \cdot \frac{1}{\left[(x(n)-\Delta x)^2 + z_p^2\right]} \\ & + a_{i2} \cdot \frac{1}{\left[(x(n))^2 + z_p^2\right]} \Bigg] \frac{z_p L}{2\pi N} \Delta H_n. \end{aligned} \tag{26}$$

$$\begin{aligned} \sum_{n=0}^{N} T_{i,n} T'_{n,j} &\approx \frac{N}{L}\left(\frac{1}{2\pi}\right)^2 \int_{x=-\infty}^{+\infty} \frac{z_p(z_p+e_z)}{\left[(x+a\Delta x)^2+(z_p+e_z)^2\right]\left[(x+b\Delta x)^2+z_p^2\right]} dx \\ &= \frac{N}{L}\left(\frac{1}{2\pi}\right)^2 \left[\pi \frac{(e_z)^2(2z_p+e_z)+(a-b)^2\Delta x^2(2z_p+e_z)}{2(a-b)\Delta x(z_p+e_z)z_p} + \ln\frac{(z_p+e_z)^2}{z_p^2}\right] \\ &\quad \times \left[\frac{2(a-b)\Delta x z_p(z_p+e_z)}{\left[(z_p+e_z)^2 - z_p^2 + (a-b)^2\Delta x^2\right]^2 + 4(a-b)^2\Delta x^2 z_p^2}\right] \end{aligned} \tag{22}$$

The average error in the currents is then zero and the variance is

$$\langle(\Delta J_1)^2\rangle = \left\langle \left(\sum_{n=0}^{N} \left[a_{i1} \times \frac{1}{[(x(n)+\Delta x)^2 + z_p^2]} + a_{i3} \times \frac{1}{[(x(n)-\Delta x)^2 + z_p^2]} + a_{i2} \times \frac{1}{[(x(n))^2 + z_p^2]} \right] \frac{z_p L}{2\pi N} \Delta H_n \right)^2 \right\rangle$$
$$= \sum_{n=0}^{N} \left[a_{i1} \times \frac{1}{[(x(n)+\Delta x)^2 + z_p^2]} + a_{i3} \times \frac{1}{[(x(n)-\Delta x)^2 + z_p^2]} + a_{i2} \times \frac{1}{[(x(n))^2 + z_p^2]} \right]^2 \left(\frac{z_p}{2\pi}\right)^2 \left(\frac{L}{N}\right)^2 \sigma^2. \quad (27)$$

Assuming the sampling density is high enough to allow the summation to be calculated through integration, the variance becomes

$$\left\langle (\Delta J_i)^2 \right\rangle = \left(\frac{L}{N}\right)\left(\frac{1}{8\pi z_p}\right) \left[a_{i1}^2 + a_{i2}^2 + a_{i3}^2 + (2a_{i1}a_{i2} + 2a_{i2}a_{i3}) \frac{4z_p^2}{[\Delta x^2 + 4z_p^2]} + 2a_{i1}a_{i3} \frac{z_p^2}{[\Delta x^2 + z_p^2]} \right] \sigma^2. \quad (28)$$

As shown earlier, the variance in the error in inferred currents is directly proportional to the sampling density, L/N, and the noise, σ^2. The smaller the sampling density and the smaller the noise, the lower the variance in the resulting errors. The ill-posed nature of this problem, however, may significantly exaggerate the noise as the values of a_{i1}, a_{i2}, and a_{i3} may be large. The error can be reduced by limiting the measurement area (L) to only those locations where the signal from the device under test is significant compared to the noise floor of the instrumentation.

Errors in inferred currents are also a function of the spacing between adjacent traces, Δx, and the height of the probe, z_p. To illustrate, the error in inferred currents due to random noise in measured magnetic fields is plotted in Figs. 24 and 25 as a function of the distance between the traces and the height of the probe. Here, the default values for intersample spacing and variance in measured noise are $dx = 0.1\,\text{mm}$, $\sigma^2 = 1$. In general, the greater the spacing between the traces and the lower the height of the probe, the better the estimated currents.

To test the influence of errors in the dielectric constant, transmission line simulations of the near-magnetic field over a microstrip trace were performed while varying the size of the dielectric constant. The configuration of the microstrip trace is shown in Fig. 26. Its overall length was 2 cm. One simulation was performed at 100 MHz when the dielectric material had a dielectric constant equivalent to free space and one simulation

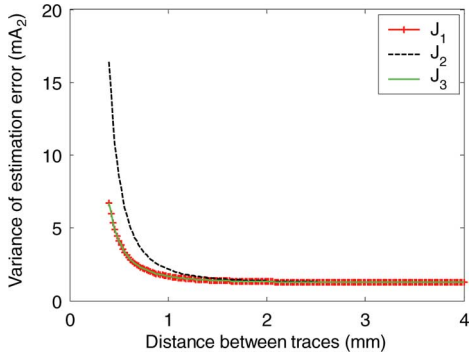

Fig. 24. Error in inferred currents J_1, J_2, and J_3 caused by random noise as a function of distance between the traces.

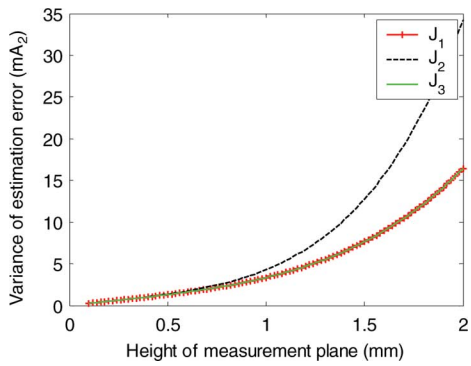

Fig. 25. Error in inferred currents J_1, J_2, and J_3 caused by random noise as a function of distance between the traces and the measurement plane.

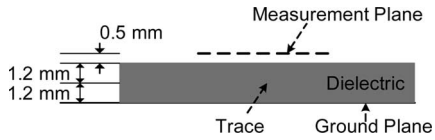

Fig. 26. Structure used to test the influence of the dielectric constant.

was performed when the dielectric constant was equivalent to that of FR4. The difference in the resulting near-magnetic fields was less than 1%, indicating that the dielectric constant will not be important for traces buried in the package lead frame or PCB at frequencies where the circuit is electrically small. When displacement current becomes important, however, the dielectric constant can play an important role in the accuracy of the inferred currents, as indicated in Section III-E.

V. Conclusion

Near-field scan data may be used to infer high-frequency currents in PCB traces and in the package lead frame, even when the currents are buried in the PCB or package. This technique allows one to estimate currents that may be difficult or impossible to find with other techniques or that may require development of specialized test boards. The accuracy of the inferred currents is dependent on the accuracy of geometry information and the measurement. Knowledge about the location of current-carrying traces can be used to constrain inverse solutions. While current distributions can be inferred even without trace information, results are better when this information is available. With trace information and errors typical to the measurement process, currents can be estimated in a typical measurement

setup to within an average of 20% (1.6 dB) or less of their correct value. Better current estimates can be expected if the errors in probe position or measurement noise are reduced or if the probe is placed closer to the device under test. Here it was assumed the probe height was 1.7 mm and there was a 0.2 mm error in the horizontal or vertical position of the probe, there was a 15 degree error in probe rotation, or there was 20% measuremet noise. Reductions in these errors or in probe height are practical with currently available technology by calibrating the position of the probe relative to the device under test, by using narrowband measurement techniques, and by using small probes and placing them close to the current-carrying wires. While average errors may increase as the density of the current-carrying wires increases beyond the 20-pin dual in-line package studied here, the effect may be mitigated using smaller probes placed close to the current-carrying wires. Average errors in estimated currents less than 20% should be reasonable in many practical applications.

REFERENCES

[1] N. Masuda, N. Tamaki, H. Wabuka, T. Watanable, and K. Ishizaka, "RF current evaluation of ICs by MP-10 L," *NEC R&D*, vol. 40, no. 2, pp. 253–258, 1999.

[2] N. Masuda, N. Tamaki, H. Wabuka, T. Watanable, and K. Ishizaka, "A multilayer board-type magnetic field probe with high spatial resolution and RF current estimation method for ICs," in *Proc. IEEE Int. Symp. Electromagn. Compat.*, 1999, p. 801.

[3] W. R. Pfaff, "Application independent evaluation of electromagnetic emissions for integrated circuits by the measurement of conducted signals," in *Proc. IEEE Int. Symp. Electromagn. Compat.*, Denver, CO, 1998, pp. 340–345.

[4] Cookbook for integrated circuit model ICEM, [Online]. Available: http://www.eseo.fr/∼mramdani/cookbook.pdf

[5] *Integrated Circuits—Measurement of Electromagnetic Emissions, 150 kHz to 1 GHz—Part 6: Measurement of Conducted Emissions, Magnetic Probe Method*, IEC Standard 61967-6, 2002.

[6] F. Fiori and F. Musolino, "Measurement of integrated circuit conducted emissions by using a transverse electromagnetic mode (TEM) cell," *IEEE Trans. Electromagn. Compat.*, vol. 43, no. 4, pp. 622–628, Nov. 2001.

[7] X. Dong, S. Deng, D. G. Beetner, T. H. Hubing, and T. P. Van Doren, "Determination of high frequency package currents from near-field scan data," in *Proc. IEEE Symp. Electromagn. Compat.,* Aug. 8–12, 2005, pp. 679–683.

[8] A. D. Yaghjian, "An overview of near-field antenna measurements," *IEEE Trans. Antennas Propag.*, vol. AP-34, no. 1, pp. 30–45, Jan. 1986.

[9] K. P. Slattery, J. W. Neal, and W. Cui, "Near-field measurements of VLSI Devices," *IEEE Trans. Electromagn. Compat.*, vol. 41, no. 4, pp. 374–384, Nov. 1999.

[10] R. D. Throne and L. G. Olson, "A generalized eigensystem approach to the inverse problem of electrocardiography," *IEEE Trans. Biomed. Eng.*, vol. 41, no. 6, pp. 592–600, Jun. 1994.

[11] R. M. Gulrajani, "The forward and inverse problems of electrocardiography," *IEEE Eng. Med. Biol. Mag.*, vol. 17, no. 5, pp. 84–101, Sep. 1998.

[12] D. G. Beetner and R. M. Arthur, "Direct inference of the spectra of pericardial potentials using the boundary-element method," *Ann. Biomed. Eng.*, vol. 27, pp. 498–507, 1999.

[13] C. A. Balanis, *Advanced Engineering Electromagnetics*. New York: Wiley, 1989.

[14] B. J. Messinger-Rapport and Y. Rudy, "The inverse problem in electrocardiography: A model study of the effects of geometry and conductivity parameters on the reconstruction of epicardial potentials," *IEEE Trans. Biomed. Eng.*, vol. BME-33, no. 7, pp. 667–676, Jul. 1986.

[15] T. Stadtler, L. Eifler, and J. L. ter Haseborg, "Double probe near field scanner, a new device for measurements in time domain," in *Proc. 2003 IEEE Symp. Electromagn. Compat.*, Boston, MA, Aug. 18–22, pp. 86–90.

[16] J. Shi, M. A. Cracraft, K. P. Slattery, M. Yamaguchi, and R. E. DuBroff, "Calibration and compensation of near-field scan measurements," *IEEE Trans. Electromagn. Compat.*, vol. 47, no. 3, pp. 642–650, Aug. 2005.

[17] *74FCT807 T Data Sheet*, Integrated Device Technology, Inc., San Jose, CA. Dec. 2000.

[18] K. Hu, H. Weng, D. G. Beetner, D. Pommerenke, J. Drewniak, K. Lavery, and J. Whiles, "Application of chip-level EMC in automotive product design," in *Proc. IEEE Symp. Electromagn. Compat.,* Portland, OR, vol. 3, Aug. 2006, pp. 842–848.

[19] N. Masuda, N. Tamaki, T. Kuriyama, B. J. Ching, M. Yamaguchi, and K. Arai, "High frequency magnetic near field measurement on LSI chip using planar multi-layer shielded loop coil," in *Proc. IEEE Symp. Electromagn. Compat.*, Boston, MA, Aug. 18–22, 2003, pp. 80–85.

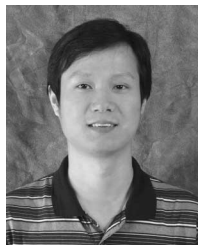

Haixiao Weng (M'02) was born in JiangYan, China, on March 18, 1976. He received the B.Sc. and M.Sc. degrees in electrical engineering from Tsinghua University, Beijing, China, in 1998 and 2000, respectively, and the Ph.D. degree from the University of Missouri-Rolla, Rolla, in 2006.

He is currently with Texas Instruments, Inc., Dallas, TX.

Daryl G. Beetner (S'89–M'98–SM'03) received the B.S. degree from Southern Illinois University, Edwardsville, in 1990, and the M.S. and D.Sc. degrees from Washington University, St. Louis, MO, in 1994 and 1997, respectively, all in electrical engineering.

He is currently an Associate Professor of electrical and computer engineering at the University of Missouri-Rolla, Rolla, where he is also the Associate Chair of the Computer Engineering Program. His current research interests include a wide range of topics including skin cancer detection, humanitarian demining, very large scale integrated circuit design, and electromagnetic compatibility.

Richard E. DuBroff (S'74–M'74–SM'84) received the B.S.E.E. degree from Rensselaer Polytechnic Institute, Troy, NY, in 1970, and the M.S. and Ph.D. degrees in electrical engineering from the University of Illinois, Urbana-Champaign, in 1972 and 1976, respectively.

From 1976 to 1978, he was a Postdoctoral Fellow in the Ionosphere Radio Laboratory, University of Illinois, where he was engaged in research on backscatter inversion of ionospheric electron density profiles. From 1978 to 1984, he was a Research Engineer in the Geophysics Branch, Phillips Petroleum, Bartlesville, OK. Since 1984, he has been with the University of Missouri-Rolla, Rolla, where he is currently a Professor in the Department of Electrical and Computer Engineering.

Jin Shi (S'00–M'00) was born in China in 1974. He received the B.S.E.E. degree from the Central South University, Changsha, China, in 1997, the M.S. degree in electrical engineering from Tsinghua University, Beijing, China, in 2000, and the Ph.D. degree in electrical engineering from the University of Missouri-Rolla, Rolla, in 2005.

Since 2000, he has been with the Electromagnetic Compatibility Laboratory, University of Missouri-Rolla, where his research and education have been supported by a research assistantship. Since January 2005, he has also been a Senior Hardware Engineer with the Mobile Platform Group, Intel Corporation, Santa Clara, CA. His current research interests include EMI/RFI and signal/power integrity issues in high-speed digital systems.